EURANDOM PREPRINT SERIES
2010-030

Modeling of Electrochemical Hydrogen Storage in Metal Hydride Electrodes

A. Ledovskikh, D. Danilov, P. Vermeulen, P.H.L. Notten
ISSN 1389-2355

Modeling of Electrochemical Hydrogen Storage in Metal Hydride Electrodes

A. Ledovskikh[1], D. Danilov[2], P. Vermeulen[2] and P.H.L. Notten[2]

[1] *Eurandom, Den Dolech 2, 5600 MB Eindhoven, The Netherlands*

[2] *Eindhoven University of Technology, Den Dolech 2, 5600 MB Eindhoven, The Netherlands*

The recently presented Electrochemical Kinetic Model (EKM), describing the electrochemical hydrogen storage in hydride-forming materials, has been extended by the description of the solid/electrolyte interface, *i.e.* the charge transfer kinetics and electrical double layer charging. A complete set of equations has been derived, describing the equilibrium hydrogen partial pressure, the equilibrium electrode potential, the exchange current density and the electrical double layer capacitance as a function of hydrogen content in both solid-solutions and two-phase coexistence regions. The model has been applied to simulate isotherms of Pd thin films with a nominal thickness of 200 and 10 nm. The model demonstrates good agreement between the simulation results and experimental data.

I. INTRODUCTION

Nowadays modern civilization faces the hazardous global warming which is a result of consumption of traditional fossil fuels. To decrease CO_2 emission sharp improvements in energy generation technologies are required. Modern society urgently needs more sustainable energy. It is commonly accepted that electricity storage systems are the key element of energy efficient technologies and hydrogen is considered as one of the most important future energy carriers. High energy density rechargeable nickel metal hydride (NiMH) batteries which are based on principles of electrochemical hydrogen storage play an important role in modern industrial, automotive and portable electronics sectors. These batteries are relatively cheap, ecologically friendly and have advantages over other types of batteries especially in transportation and automotive applications. To control operation of hybrid electrical vehicles (HEV) nowadays and plug-in electrical vehicles (PEV) in the future, new effective generation of battery management systems (BMS) is required [1-5].

The core of the modern BMS is a mathematical model of applied battery. Therefore modeling of the NiMH battery is important for safe and efficient operation of HEV and PEV. On the other hand modeling of such complex electrochemical system as the NiMH battery is also interesting from scientific point of view. It gives more insight into complex hydrogen storage process and, therefore, interesting for material scientists and battery designers.

As a first step of the NiMH battery modeling, a new thermodynamic Lattice Gas Model (LGM) describing the thermodynamics of hydrogen storage has recently been developed [6-8]. A number of microscopic parameters, such as interaction energies between absorbed hydrogen atoms, can be obtained by fitting the experimental data. The LGM demonstrated a good agreement with the experimental results of various hydride-forming materials. However, this model does not consider the kinetics of (de)hydrogenation.

As a next step a Kinetic Model (KM) of hydrogen storage was developed, which describes the equilibrium kinetics of hydrogen storage via the gas phase [9]. KM is based on the principles of statistical thermodynamics, described in LGM [6-8], and also takes into account the complex gas phase (de)hydrogenation kinetics. The advantage of this kinetic approach is that it can, in principle, describe both equilibrium and non-equilibrium (dynamic) conditions. In the equilibrium state, the kinetic approach has, however, to comply with the thermodynamics [10]. Combining the thermodynamics and kinetics was shown to offer an interesting opportunity to estimate not only the hydrogen storage-related

thermodynamic parameters but also the relevant kinetic reaction rates and rate constants [9,11].

Finally, an Electrochemical Kinetic Model (EKM) was developed, describing the electrochemical hydrogen storage in hydride-forming materials under equilibrium conditions [12]. This model was proposed as an extension of the KM [9] and is also based on the first principles of electrochemical reaction kinetics and statistical thermodynamics and describes the complex, multi-stage, electrochemical (de)hydrogenation process. A complete set of equations has been derived, describing the equilibrium hydrogen partial pressure and equilibrium electrode potential as a function of hydrogen content in both solid-solution and two-phase coexistence regions [12]. All above models have been successfully applied to simulate the isotherms of various hydride-forming materials, including AB_5-based and Mg-based alloys [6-9,11-13].

In the present paper a further extension of the EKM is proposed to include the dynamic electrochemical (de)hydrogenation kinetics, *i.e.* to include the exchange current density of the charge transfer reaction, electrical double layer charging and (instantaneous) phase transition. The electrode/electrolyte interface properties will be described by conventional electrochemical parameters, *i.e.* by the exchange current density and specific electrical double layer capacitance. As has been theoretically shown and experimentally proven the charge transfer kinetics is a function of the hydrogen content inside the solid [14,15]. The performance of the model is illustrated with results obtained with thin film Pd electrodes [7], which were used before to identify parameters of the EKM [12].

II. EXPERIMENTAL

Palladium thin films, with a nominal thickness of 10 and 200 nm were deposited on quartz substrates (diameter 20 mm) by means of electron beam deposition. A 1 nm thick Gd-layer was deposited onto the substrate prior to Pd deposition to enforce good adhesion. The base pressure during deposition was between 1×10^{-7} and 1×10^{-6} mbar. The film thickness was measured by Rutherford backscattering (RBS).

A standard three-electrode electrochemical setup was used to characterize the hydrogen absorption/desorption characteristics of the Pd electrodes. The set-up was thermostated at 298 K by means of a water jacket surrounding the cell and filled with 6 M KOH electrolyte. The potential of the Pd working electrode was monitored *versus* a lead-free

Hg/HgO reference electrode (Koslow Scientific Company, USA) [16]. The counter electrode was a palladium rod that was placed in a separate compartment of the cell and care was taken that the surface area in contact with the electrolyte was sufficiently large. The compartments were separated by means of fritted glass. In a separate set-up the counter electrode was pre-charged with hydrogen to form PdH_x. The total amount of charge needed to extract all the hydrogen from this palladium rod far exceeded the charge needed to fully hydrogenate the working electrode. This ensured that during the electrochemical experiments no oxygen was produced at the palladium counter electrode.

Prior to the experiment the electrolyte was de-aerated by purging for 1 hour with a continues O_2-free argon-flow as it is known that even small amounts of O_2 can seriously affect the hydrogen content and the electrochemical potential of thin film electrodes [17]. Special care was taken to remove oxygen traces from the argon feed by passing the gas stream through a Viologen scrubber just before entering the gas-tight electrochemical cell.

The isotherms of Pd thin film electrodes were determined by conducting Galvanostatic Intermittent Titration Technique (GITT) measurements using an Autolab PGSTAT30 (Ecochemie B.V., The Netherlands). Because the recombination reaction (later to be identified as Eq. (4)) might compete with the hydrogenation reaction (see Eq. (2)) it can lead to inaccuracies in the calculated amount of hydrogen that is assumed to be absorbed. Therefore all isotherms presented in this paper are obtained during dehydrogenation only, which do not suffer from the competing recombination reaction. The Pd thin films were galvanostatically fully charged using a reduction current of -0.12 mA, except for the 10 nm thick Pd electrode for which a current of -0.012 mA was used. Hereafter, the electrodes were allowed to equilibrate for 1 h. The PdH_x electrodes were subsequently discharged by means of GITT in approximately 20 pulses using an oxidation current of +0.012 mA for the 10 nm thick Pd film, whereas for the thicker Pd films a current of +0.12 mA was used. A 1 hour equilibration period was used after each current pulse to ensure a constant electrochemical potential. To prevent the formation of O_2, a 0 V cut-off voltage was applied during the galvanostatic hydrogen extraction experiments. All electrochemical potentials are given with respect to Hg/HgO (6 M KOH). Note that the ultra-thin Gd adhesion layer is assumed not to influence the electrochemical response as it is known that films of less than 3 mono-layers do not absorb any appreciable amount of hydrogen [18,19].

In order to obtain detailed information about the charge transfer kinetics and double layer capacitance of the MH electrodes as a function of hydrogen content, Electrochemical Impedance Spectroscopic (EIS) measurements have been carried out under equilibrium conditions at the end of each relaxation period along the electrochemically determined isotherms. The impedance measurements have been performed with a sinusoidal potential perturbation of 5 mV within the frequency range of 1 mHz to 10 kHz. The EIS-data have been fitted to an equivalent circuit using standard software (EQUIVCRT) [20].

III. MODEL

A. General description of the electrochemical MH-system

A detailed derivation of the EKM as a basis of the present model extension can be found in [12]. The present paper follows the same definitions and notations. The cornerstones of the EKM will be taken as starting point and will be represented below for the reader convenience.

A schematic representation of the electrochemical hydrogen storage processes, including phase transition (hydrogen poor α- and hydrogen rich β-phase solid-solution regions and α-to-β two-phase coexistence region), is represented in Fig. 1a. After the charge-transfer reaction at the electrode/electrolyte interface of the hydride-forming material (M^s) has been initiated, atomic hydrogen is chemically adsorbed (H_{ad}) at the electrode surface and is, subsequently, converted into the absorbed state (H_{abs}) and transported to the bulk of the hydride-forming material (M^b) by means of conventional solid state diffusion [9,12,21]. In Fig. 1, the normalized hydrogen concentration in the bulk of the MH electrode is represented by x and the normalized surface concentration by θ, which is also known as the surface coverage. Alternatively, two adsorbed hydrogen can recombine at the electrode surface which results in molecular hydrogen dissolved in the electrolyte (H_2^l) at concentration c_l. Obviously, dissolved molecular hydrogen is in equilibrium with that in the gas phase (H_2^g) at concentration c_g. The complete electrochemical hydrogen storage process, taking place at/in the MH electrode and the

accompanying reaction fluxes are schematically represented in Fig. 1b and consists of four different steps [12]:

(*i*) Hydrogen dissociation/recombination at the electrode/electrolyte interface

$$2M^s + H_2^l \underset{k_{-1}}{\overset{k_1}{\rightleftharpoons}} 2M^sH_{ad} \quad (1)$$

(*ii*) Hydrogen absorption/desorption in the bulk of the MH-electrode

$$M^b + M^sH_{ad} \underset{k_{-2}}{\overset{k_2}{\rightleftharpoons}} M^bH_{abs} + M^s \quad (2)$$

(*iii*) Charge-transfer at the electrode/electrolyte interface

$$M^s + H_2O + e^- \underset{k_{-3}}{\overset{k_3}{\rightleftharpoons}} M^sH_{ad} + OH^- \quad (3)$$

(*iv*) Molecular hydrogen exchange between the electrolyte and the gas phase

$$H_2^l \underset{k_{-4}}{\overset{k_4}{\rightleftharpoons}} H_2^g \quad (4)$$

According to the general reaction scheme (Fig 1a), the system under consideration consists of three regions, corresponding to the gas phase, the electrode/electrolyte interface (electrode surface) and the bulk of the hydride-forming material. Taking phase separation into account it is assumed that the reactions described by Eqs. 1-3 take place separately at/in each phase. This also holds for the reaction fluxes, which are assumed to flow independently in all distinct regions of the system (Fig. 1b). For the sake of consistency, the numeration represented in Eqs. 1-4, has been kept in line with the definitions and notations used before [6-9,11-13]. The following set of reaction flux equations has been derived (see Fig. 1b) [12]:

(*i*) Mathematical description of the hydrogen absorption/desorption reaction at the surface of the hydride-forming material (Eq. 2). This set of equations expresses the basic relationship between the hydrogen concentration in the bulk of the MH electrode and the

surface coverage for the α-phase (Eq. 5a) and β-phase (Eq. 5b) in both solid-solution and two-phase coexistence region, according to

$$\begin{cases} \dfrac{x(1-\theta)}{\theta(1-x)} = \mathrm{B}_2^{\alpha} \exp\left(\dfrac{E_{\alpha}^{s} + U_{\alpha\alpha}^{s}\theta - (E_{\alpha}^{b} + U_{\alpha\alpha}^{b}x)}{(RT/F)} \right), & 0 \le x < \mathrm{x}_{\alpha} \\ \dfrac{x_{\alpha}(1-\theta_{\alpha})}{\theta_{\alpha}(1-x_{\alpha})} = \mathrm{B}_2^{\alpha} \exp\left(\dfrac{E_{\alpha}^{s} + U_{\alpha\alpha}^{s}\theta^{\alpha}}{(RT/F)} - H_x(x) \right), & \mathrm{x}_{\alpha} \le x \le \mathrm{x}_{\beta} \end{cases} \tag{5a}$$

$$\begin{cases} \dfrac{x_{\beta}(1-\theta_{\beta})}{\theta_{\beta}(1-x_{\beta})} = \mathrm{B}_2^{\beta} \exp\left(\dfrac{E_{\beta}^{s} + U_{\beta\beta}^{s}\theta^{\beta}}{(RT/F)} - H_x(x) \right), & \mathrm{x}_{\alpha} \le x \le \mathrm{x}_{\beta} \\ \dfrac{x(1-\theta)}{\theta(1-x)} = \mathrm{B}_2^{\beta} \exp\left(\dfrac{E_{\beta}^{s} + U_{\beta\beta}^{s}\theta - (E_{\beta}^{b} + U_{\beta\beta}^{b}x)}{(RT/F)} \right), & \mathrm{x}_{\beta} < x \le 1 \end{cases} \tag{5b}$$

where $H_x(x) = \dfrac{F}{RT(\mathrm{x}_{\beta} - \mathrm{x}_{\alpha})}(E_{\beta}^{b}\mathrm{x}_{\beta} - E_{\alpha}^{b}\mathrm{x}_{\alpha} - U_{\alpha\alpha}^{b}\mathrm{x}_{\alpha}^{2}\dfrac{N_{\alpha}^{b}}{n_{\max}^{b}} + U_{\beta\beta}^{b}\mathrm{x}_{\beta}^{2}\dfrac{N_{\beta}^{b}}{n_{\max}^{b}} + U_{\alpha\beta}^{b}\mathrm{x}_{\alpha}\mathrm{x}_{\beta}(\dfrac{N_{\alpha}^{b}}{n_{\max}^{b}} - \dfrac{N_{\beta}^{b}}{n_{\max}^{b}})/2 + L)$,

B_2^i are the combined pre-exponential factors, dependent on the frequency of atomic collisions of the forward (absorption) and backward (desorption) reactions in phases $i\,(i = \alpha, \beta)$, E_i^j are the energies of the individual hydrogen atoms in phase i and region j ($j = s, b$ at the surface (s) or in the bulk (b)), U_{ii}^j is the interaction energies between hydrogen atoms within each phase i, $U_{\alpha\beta}^b$ the inter-phase interaction energy between hydrogen atoms located in different phases of the hydride-forming material, R the gas constant, T the temperature, F the Faraday constant, x_i the phase transition points or critical concentration of hydrogen at which phase transition of the hydride-forming material is started/ended, N_i^j the total number of available host sites at which hydrogen atoms can be adsorbed in region j and phase i, $n_{\max}^j$ the total number of available host sites in region j, $L = L_{\beta} - L_{\alpha}$ is the difference between energy levels of the crystal lattice of β-phase (L_{β}) and α-phase (L_{α}) and x_i and θ_i are the phase-normalized hydrogen concentrations in the bulk and at the surface, respectively, which has been defined as [9,12]

$$x_i = \frac{n_i^b}{N_i^b}; \quad \theta_i = \frac{n_i^s}{N_i^s} \tag{6}$$

in which n_i^b is the number of hydrogen atoms located in the phase *i* and the partial surface coverage (θ^i) can be calculated from

$$\theta^i = \frac{n_i^s}{n_{\max}^s} \tag{7}$$

(*ii*) Set of equations, describing the equilibrium hydrogen pressure ($P_{H_2}^{eq}$), has been derived from the description of the dissociation/recombination reactions (Eq. 1) and hydrogen exchange reaction between the electrolyte and gas phase (Eq. 4) [12]. An analytical solution is obtained, which expresses the equilibrium partial hydrogen pressure in the three distinct crystallographic regions as a function of the hydrogen concentration in the bulk of the hydride-forming material and various surface coverage's and rate constants, according to

$$P_{H_2}^{eq} = \begin{cases} P_\alpha \left(\dfrac{x}{1-x}\right)^2 \exp\left(2\dfrac{E_\alpha^b + U_{\alpha\alpha}^b x}{(RT/F)}\right), & 0 \le x < \mathrm{x}_\alpha \\ \dfrac{P_\alpha \dfrac{x_\alpha^2 (1-\theta_\alpha)^2}{(1-x_\alpha)^2}\dfrac{N_\alpha^b}{n_{\max}^b} + P_\beta \dfrac{x_\beta^2 (1-\theta_\beta)^2}{(1-x_\beta)^2}\dfrac{N_\beta^b}{n_{\max}^b}}{(1-\theta_\alpha)^2 \dfrac{N_\alpha^b}{n_{\max}^b} + (1-\theta_\beta)^2 \dfrac{N_\beta^b}{n_{\max}^b}} \exp\left(2H_x(x)\right), & \mathrm{x}_\alpha \le x \le \mathrm{x}_\beta \\ P_\beta \left(\dfrac{x}{1-x}\right)^2 \exp\left(2\dfrac{E_\beta^b + U_{\beta\beta}^b x}{(RT/F)}\right), & \mathrm{x}_\beta < x \le 1 \end{cases} \tag{8}$$

where P_i is a combined parameter expressed as

$$P_i = RTK_4 \frac{\mathrm{B}_1^i}{\left(\mathrm{B}_2^i\right)^2} \exp\left(\frac{\varepsilon_l}{(RT/F)}\right) \tag{9}$$

K_4 is the dimensionless Henry's constant; B_1^i are pre-exponential factors, which depend on the frequency of atomic collisions of the forward (dissociation) and backward (recombination) reactions (Eq. 1) in phase i; $\varepsilon_l = \frac{5}{2}kT$ is the energy of a single hydrogen molecule dissolved in the electrolyte; k is Bolzmann's constant [12].

(*iii*) Set of equations, describing the equilibrium potential of the MH electrode (E_{MH}^{eq}), has been derived from the charge-transfer reaction (Eq. 3). An analytical solution is obtained, which expresses the equilibrium potential of the MH electrode in the three distinct crystallographic regions as a function of the hydrogen concentration in the bulk of the hydride-forming material and various surface coverage's and rate constants, according to [12]:

$$E_{MH}^{eq} = \begin{cases} \dfrac{RT}{F}\ln\left(\dfrac{1-x}{x}\right) + \dfrac{RT}{F}\ln(E_{\alpha}^{0}) - E_{\alpha}^{b} - U_{\alpha\alpha}^{b}x, & 0 \le x < \mathrm{x}_{\alpha} \\ \dfrac{RT}{F}\ln\left(\dfrac{E_{\alpha}^{0}\exp\left(U_{\alpha\alpha}^{s}\theta^{\alpha}\right)\dfrac{\theta_{\alpha}(1-x_{\alpha})}{x_{\alpha}} + E_{\beta}^{0}\exp\left(U_{\beta\beta}^{s}\theta^{\beta}\right)\dfrac{\theta_{\beta}(1-x_{\beta})}{x_{\beta}}}{\exp\left(U_{\alpha\alpha}^{s}\theta^{\alpha}\right)\theta_{\alpha} + \exp\left(U_{\beta\beta}^{s}\theta^{\beta}\right)\theta_{\beta}}\right) - H_{x}(x), & \mathrm{x}_{\alpha} \le x \le \mathrm{x}_{\beta} \\ \dfrac{RT}{F}\ln\left(\dfrac{1-x}{x}\right) + \dfrac{RT}{F}\ln(E_{\beta}^{0}) - E_{\beta}^{b} - U_{\beta\beta}^{b}x, & \mathrm{x}_{\beta} < x \le 1 \end{cases} \tag{10}$$

where E_i^0 is a combined parameter expressed as

$$E_i^0 = \mathrm{B}_2^i \mathrm{B}_3^i \exp\left(\frac{\varepsilon_{H_2O}}{(RT/F)}\right) \tag{11}$$

B_3^i are pre-exponential factors and $\varepsilon_{H_2O} \approx 3.233kT$ is the energy of a hydrogen atom in a water molecule [12].

B. Exchange current density and specific electrical double layer capacitance

The forward (j_3^i) and backward (j_{-3}^i) normalized charge-transfer fluxes of the electrochemical reaction (Eq. 3) has been described in [12] as

$$\begin{cases} j_3^i = k_3^i(1-\theta_i)(N_i^b / n_{\max}^b) \\ j_{-3}^i = k_{-3}^i\theta_i(N_i^b / n_{\max}^b) \end{cases} \tag{12}$$

By adopting the so-called electrochemical rectangular rule [12] the reaction rate constants can be related to the activation potential barrier of the charge-transfer process (Π_{ca}), the energies of reacting species (ε_{H_2O}, ε_θ^i) and the equilibrium potential of the MH electrode (E_{MH}^{eq}), according to

$$\begin{cases} k_3^i = B_3^i \exp\left(-\dfrac{\Pi_{ca}}{kT}\right)\exp\left(\dfrac{\varepsilon_{H_2O} - \alpha e E_{MH}^{eq}}{kT}\right) \\ k_{-3}^i = B_{-3}^i \exp\left(-\dfrac{\Pi_{ca}}{kT}\right)\exp\left(\dfrac{\varepsilon_\theta^i + (1-\alpha) e E_{MH}^{eq}}{kT}\right) \end{cases} \tag{13}$$

where B_3^i and B_{-3}^i are the forward and backward reaction pre-exponential factors, respectively, corresponding to phase *i*; α the charge-transfer coefficient (assumed to be identical for the α- and β-phase in this work) and *e* is the elemental charge. ε_θ^i has been defined as $\varepsilon_\theta^i = E_i^s + U_{ii}^s \theta^i$ [9,12].

According to [22] the net charge transfer current density can be expressed by the difference between forward and backward charge-transfer reaction fluxes as

$$i = nF(j_3 - j_{-3}) \tag{14}$$

in which the number of electrons (*n*) involved in the present charge-transfer process is unity, according to reaction Eq. 3. Under equilibrium conditions the following general flux balances hold

$$\begin{cases} j_3^\alpha = j_{-3}^\alpha, & 0 \le x < \mathrm{x}_\alpha \\ j_3^\alpha + j_3^\beta = j_{-3}^\alpha + j_{-3}^\beta, & \mathrm{x}_\alpha \le x \le \mathrm{x}_\beta \\ j_3^\beta = j_{-3}^\beta, & \mathrm{x}_\beta < x \le 1 \end{cases}, \tag{15}$$

Combining the flux balances of Eqs. 15 with Eqs. 12-14 yields the exchange current density. The cathodic (i_c^0) and anodic (i_a^0) exchange current densities can then be expressed as

$$i_c^0 = F\exp\left(-\frac{\Pi_{ca}}{kT}\right)\exp\left(\frac{(1-\alpha)FE_{MH}^{eq}}{RT}\right)\begin{cases}\theta\exp\left(\dfrac{E_\alpha^s+U_{\alpha\alpha}^s\theta}{(RT/F)}\right), & 0\le x<\mathrm{x}_\alpha\\ \exp\left(\dfrac{E_\alpha^s+U_{\alpha\alpha}^s\theta^\alpha}{(RT/F)}\right)\theta_\alpha(N_\alpha^b/n_{\max}^b)+\exp\left(\dfrac{E_\beta^s+U_{\beta\beta}^s\theta^\beta}{(RT/F)}\right)\theta_\beta(N_\beta^b/n_{\max}^b), & \mathrm{x}_\alpha\le x\le\mathrm{x}_\beta\\ \theta\exp\left(\dfrac{E_\beta^s+U_{\beta\beta}^s\theta}{(RT/F)}\right), & \mathrm{x}_\beta<x\le 1\end{cases} \quad (16.a)$$

$$i_a^0 = F\exp\left(-\frac{\Pi_{ca}}{kT}\right)\exp(3.233)\exp\left(-\frac{\alpha FE_{MH}^{eq}}{RT}\right)\begin{cases}\mathrm{B}_3^\alpha(1-\theta), & 0\le x<\mathrm{x}_\alpha,\\ \mathrm{B}_3^\alpha(1-\theta_\alpha)(N_\alpha^b/n_{\max}^b)+B_3^\beta(1-\theta_\beta)(N_\beta^b/n_{\max}^b), & \mathrm{x}_\alpha\le x\le\mathrm{x}_\beta,\\ \mathrm{B}_3^\beta(1-\theta), & \mathrm{x}_\beta<x\le 1.\end{cases} \quad (16.b)$$

respectively. Obviously, both exchange current densities are equal by definition ($i_c^0 = i_a^0$).

It is generally accepted that the electrical double layer can be described by a simple capacitor, especially when the diffuse double layer can be considered negligibly small in concentrated electrolytes [22,23]. Referring to Fig. 1, it is obvious that the electrical double layer of the present MH electrode can have up to four different components: both the α- and β-phase can either be covered or uncovered by adsorbed hydrogen. The specific electrical double layer capacitance can, in the simplest case, be represented by

$$C_{MH}^d = \varepsilon\varepsilon_0\begin{cases}\dfrac{\theta}{d_\theta^\alpha}+\dfrac{1-\theta}{d_{1-\theta}^\alpha}, & 0\le x<\mathrm{x}_\alpha\\ \left[\dfrac{\theta_\alpha}{d_\theta^\alpha}+\dfrac{1-\theta_\alpha}{d_{1-\theta}^\alpha}\right]\dfrac{N_\alpha}{n_{\max}}+\left[\dfrac{\theta_\beta}{d_\theta^\beta}+\dfrac{1-\theta_\beta}{d_{1-\theta}^\beta}\right]\dfrac{N_\beta}{n_{\max}}, & \mathrm{x}_\alpha\le x\le\mathrm{x}_\beta\\ \dfrac{\theta}{d_\theta^\beta}+\dfrac{1-\theta}{d_{1-\theta}^\beta}, & \mathrm{x}_\beta<x\le 1\end{cases} \quad (17)$$

where ε is dielectric constant, $\varepsilon_0 = 8.85419\cdot10^{-12}\,[F\,m^{-1}]$; d_θ^i and $d_{1-\theta}^i$ ($i=\alpha, \beta$) are the double layer thicknesses [nm], corresponding to the covered and uncovered surface of the α- and β-phase, respectively.

Conclusively, using first-principles of statistical thermodynamics, energy conservation laws and chemical reaction kinetics, the microscopic characteristics of hydrogen storage materials can be related to macroscopic system characteristics. Macroscopic parameters (temperature, equilibrium pressure, equilibrium potential, exchange current density, electrical double layer capacitance) can, in general, well been experimentally determined. On the other hand, microscopic parameters (hydrogen interaction energies, rate constants, potential barriers) can in general not easily been assessed. However, by simulating the

model with respect to the available experimental data these parameters can now be analyzed in detail.

C. Instantaneous phase transitions

The isotherms of conventional hydrogen storage materials under ambient conditions normally reveal a plateau, which corresponds to the two-phase coexistence region [1-3]. If the material is subjected to more extreme conditions, for example, by raising the temperature above the critical temperature [24] or the electrode thickness below the as-denoted critical thickness [7], the miscibility gap disappears. Such instantaneous phase transitions have also been observed with non-stoichiometric MH materials beyond the as-introduced critical composition like, for example, $LaNi_{5.0}Cu_{1.0}$ and has been experimentally verified by *in situ* XRD measurements [6,9].

The absence of phase transition implies that only two solid-solution regions can be discerned and that a two-phase coexistence region does not exist, *i.e.* $x_\alpha = x_\beta$ [6]. Therefore a new parameter x_{tr} has been introduced which indicates this special phase transition point [6]. Eqs. 5, 8, 10, 16 and 17 can then be rewritten as

(*i*) The hydrogen absorption/desorption reactions

$$\frac{x(1-\theta)}{\theta(1-x)} = \begin{cases} B_2^{\alpha} \exp\left(\dfrac{E_\alpha^s + U_{\alpha\alpha}^s \theta - (E_\alpha^b + U_{\alpha\alpha}^b x)}{(RT/F)} \right), & x < x_{tr} \\ B_2^{\beta} \exp\left(\dfrac{E_\beta^s + U_{\beta\beta}^s \theta - (E_\beta^b + U_{\beta\beta}^b x)}{(RT/F)} \right), & x \geq x_{tr} \end{cases} \tag{18}$$

(*ii*) The equilibrium hydrogen partial pressure

$$P_{H_2}^{eq} = \left(\frac{x}{1-x} \right)^2 \begin{cases} P_\alpha \exp\left(2\dfrac{E_\alpha^b + U_{\alpha\alpha}^b x}{(RT/F)} \right), & x < x_{tr} \\ P_\beta \exp\left(2\dfrac{E_\beta^b + U_{\beta\beta}^b x}{(RT/F)} \right), & x \geq x_{tr} \end{cases} \tag{19}$$

(*iii*) The electrochemical equilibrium potential

$$E_{MH}^{eq} = \frac{RT}{F}\ln\left(\frac{1-x}{x}\right) + \begin{cases} \dfrac{RT}{F}\ln(E_{\alpha}^{0}) - E_{\alpha}^{b} - U_{\alpha\alpha}^{b}x, & x < \mathrm{x}_{tr} \\ \dfrac{RT}{F}\ln(E_{\beta}^{0}) - E_{\beta}^{b} - U_{\beta\beta}^{b}x, & x \geq \mathrm{x}_{tr} \end{cases} \tag{20}$$

(*iv*) The exchange current density (derived from Eq. 16a)

$$i_c^0 = F\exp\left(-\frac{\Pi_{ca}}{kT}\right)\exp\left(\frac{(1-\alpha)FE_{MH}^{eq}}{RT}\right)\theta\begin{cases} \exp\left(\dfrac{E_{\alpha}^{s} + U_{\alpha\alpha}^{s}\theta}{(RT/F)}\right), & x < \mathrm{x}_{tr} \\ \exp\left(\dfrac{E_{\beta}^{s} + U_{\beta\beta}^{s}\theta}{(RT/F)}\right), & x \geq \mathrm{x}_{tr} \end{cases} \tag{21}$$

(*v*) The specific electrical double layer capacitance

$$C_{MH}^{d} = \varepsilon\varepsilon_0\begin{cases} \dfrac{\theta}{d_{\theta}^{\alpha}} + \dfrac{1-\theta}{d_{1-\theta}^{\alpha}}, & x < \mathrm{x}_{tr} \\ \dfrac{\theta}{d_{\theta}^{\beta}} + \dfrac{1-\theta}{d_{1-\theta}^{\beta}}, & x \geq \mathrm{x}_{tr} \end{cases} \tag{22}$$

To preserve continuity of characteristics (given by Eqs. 18-22) at the phase transition point x_{tr}, some restrictions have to be applied. Consider the set of equations, describing the desorption flux of hydrogen from the bulk to the surface of the hydride-forming material (Eqs. 44d in [9]) can be modified for the case of instantaneous phase transition into

$$j_{-2} = x(1-\theta)\begin{cases} \exp\left(\dfrac{E_{\alpha}^{b} + U_{\alpha\alpha}^{b}x}{(RT/F)}\right), & x < \mathrm{x}_{tr} \\ \exp\left(\dfrac{E_{\beta}^{b} + U_{\beta\beta}^{b}x}{(RT/F)}\right), & x \geq \mathrm{x}_{tr} \end{cases} \tag{23}$$

The following flux continuity condition at the phase transition point x_{tr} can then be obtained

$$E_{\alpha}^{b} - E_{\beta}^{b} + (U_{\alpha\alpha}^{b} - U_{\beta\beta}^{b})\mathrm{x}_{tr} = 0 \tag{24}$$

Combining Eq. 24 with Eqs. 18-20 and applying obvious normalization for the exchange current density ($E_i^s = 0$ see [9,12]) the following parameter restrictions can be obtained, which preserve the continuity of the main characteristics of the hydride-forming electrode at the phase transition point x_{tr}, according to

$$\mathrm{B}_2^{\beta} = \mathrm{B}_2^{\alpha};\ P_{\beta} = P_{\alpha};\ E_{\beta}^0 = E_{\alpha}^0;\ U_{\beta\beta}^s = U_{\alpha\alpha}^s \tag{25}$$

For the specific electrical double layer capacitance (Eq. 22) the continuity condition is given by $\lim_{x\uparrow \mathrm{x}_{tr}} C_{MH}^d(x) = \lim_{x\downarrow \mathrm{x}_{tr}} C_{MH}^d(x)$ and, for example, d_{θ}^{α} can be expressed by

$$d_{\theta}^{\alpha} = \frac{\theta_{tr} d_{1-\theta}^{\alpha} d_{1-\theta}^{\beta} d_{\theta}^{\beta}}{\theta_{tr} d_{1-\theta}^{\alpha} d_{1-\theta}^{\beta} + (1-\theta_{tr}) d_{\theta}^{\beta} (d_{1-\theta}^{\alpha} - d_{1-\theta}^{\beta})} \tag{26}$$

where θ_{tr} is the surface coverage at x_{tr} which can then numerically be calculated from Eq. 18.

Finally, application of a similar continuity condition to the total energy of hydrogen atoms absorbed in the bulk (Eq. 31 in [9]) allows estimating the difference between the energy levels of the crystal lattice of the β- and α-phases

$$L = (E_{\alpha}^b - E_{\beta}^b)\mathrm{x}_{tr} + \left(\frac{U_{\alpha\alpha}^b}{2} - \frac{U_{\beta\beta}^b}{2}\right)\mathrm{x}_{\mathrm{tr}}^2 \tag{27}$$

IV. RESULTS AND DISCUSSION

The excellent agreement between the simulated (line) equilibrium potential (electrochemical isotherm) curve (Eq. 10) and partial equilibrium hydrogen pressure (Eq. 8) and experimental data (symbols) [7,12] for a 200 nm Pd electrode at 25 ºC is shown in Fig.2. Three different regions can clearly be distinguished: a solid-solution region at low hydrogen concentration (x < 0.156), a long almost flat two-phase coexistence plateau region (0.156 ≤ x ≤ 0.664) and a solid-solution region at high concentrations (x>0.664).

The numerical values of the model parameters were obtained by non-linear least-square fitting and are presented in Table I. The model was simulated with respect to the experimentally measured set of equilibrium potentials, exchange current densities and electrical double layer capacitances. Some parameters are obtained from the thermodynamic LGM [7] and basic EKM model [12] like, for example, the phase transition points x_α and x_β. Such parameters are indicated in Table I by [a]. To avoid identification problems parameters P_α and E_α^0 were set to normal atmospheric pressure (~10^5 Pa) and 1, respectively. For the same reason $E_i^s = 0$ (see [9,12]). However, several parameters of basic EKM model are re-estimated to accommodate the additional experimental data for the exchange current density and electrical double layer capacitance. Hence B_2^α, U_{ii}^s, Π_{ca}, α, $d_{1-\theta}^i$ and d_θ^i are determined from the simulations and boldly indicated in Table I, while the remaining parameters $U_{\alpha\beta}^b$, L, B_3^i, *etc*. were obtained from the continuity conditions.

The presented model has been applied to simulate the experimental data for Pd thin films. The impedance results for the 10 nm Pd electrode are shown, as an example, in Fig. 3. The diameter of the semicircle clearly depends on the hydrogen content inside the solid [25]. This effect is especially strong in the α-phase region. The impedance data has been analyzed by the EQUIVCRT software program and yield information about the charge transfer kinetics and electrical double layer capacitances [20].

The experimental and simulated exchange current densities for a 200 nm thick Pd film as a function of the normalized hydrogen concentration are shown in Fig. 4a. A good agreement between experimental and simulation results is demonstrated for both the solid-solution and the two-phase coexistence regions. The partial exchange current densities for the α- (curve a) and β-phase (curve b) in the two-phase coexistence region are also indicated. Obviously, in the single α-phase region the exchange current density coincides with the total exchange current density (curves (c)). After the phase transition has been commenced, the fraction related to the α-phase gradually decreases in favor of the β-phase. When the phase transition is completed, only the partial exchange current density of the β-phase contributes to the total exchange current density. Analysis of the exchange current density (Eqs. 16a) shows that in the very beginning of the hydrogen storage process at low hydrogen concentration in the α-phase region the value of the exchange current density is very small and close to 0. Similar behavior can be observed at the end of

the hydrogen storage process where at very high hydrogen concentration the exchange current density steeply drops to 0 in the β-phase solid-solution region. Moreover because of the "competition" in a product $\exp\left(\frac{(1-\alpha)FE_{MH}^{eq}}{RT}\right)\theta$ a local maximum in the exchange current density can be observed in the α-phase solid-solution region. The possibility to predict and analyze the various charge transfer contributions of the complex hydrogen storage processes, which cannot be determined experimentally, is one of the benefits of the present model.

The experimental and simulated dependence of the exchange current density on the equilibrium potential of the MH electrode *vs.* Hg/HgO reference electrode is shown in Fig. 4b. These results are in line with the results reported before [14,15] for various AB_5-type materials. The charge-transfer coefficient α was found to be 0.35, which is quite close to the values (0.4-0.6) reported in [15]. The potential barrier Π_{ca}, the system has to overcome to facilitate the charge-transfer reactions (Eq. 3) was found to be 0.586 eV. Using the recently proposed "electrochemical rectangular rule" [12] the activation energy of the charge-transfer reaction can also be analyzed. Taking the middle of the plateau region (equilibrium potential $E_{MH}^{eq} \approx -0.86\,\mathrm{V}$) as an example, the activation energy was found to 0.527 eV (~51 kJ/mol).

The experimental and simulated electrical double layer capacitances as a function of the normalized hydrogen concentration are shown in Fig. 5a. A good agreement between the experimental data and simulations is found. The partial electrical double layer capacities for the α- and β-phase are also shown in curves (a) and (b), respectively. It is interesting to point out that the calculated electrical double layer thicknesses of the hydrogen-covered surfaces ($d_{\theta}^{\alpha} = 0.880$ nm and $d_{\theta}^{\beta} = 0.780$ nm) are bigger than those of the uncovered surfaces ($d_{1-\theta}^{\alpha} = 0.572$ nm and $d_{1-\theta}^{\beta} = 0.524$ nm). This result is physically intuitive because the presence of neutrally adsorbed hydrogen atoms between the electrical and ionic double layers increases the distance between the charged planes. In contrast to the exchange current density which drops sharply in the beginning and at the end of the hydrogenation process (Fig. 4a) the electrical double layer capacitances tend to level off. The saturated values can easily be calculated at $\theta = 0$ and $\theta = 1$ from Eq. 17. Assuming a dielectric constant of the electrolyte similar to that of water $\varepsilon = 78.4$ [26] these values amount to $C_{MH}^{d}\big|_{\theta=0} = 1.21\times10^{-4}$ F/cm^2 and $C_{MH}^{d}\big|_{\theta=1} = 0.90\times10^{-4}$ F/cm^2. In

Fig. 5b the same results are again plotted as a function of the electrode equilibrium potential and this further illustrates the excellent agreement between the experimental data and simulations results.

The 200 nm thick Pd electrode demonstrates a long and almost flat plateau in the two-phase coexistence region (Fig. 2) but it has been shown that by decreasing of the film thickness the plateau becomes more sloping and the miscibility gap completely disappears below the as-denoted critical thickness. For Pd thin films this was reported to be around 10 nm [7]. Fig. 6 shows a comparison of the exchange current densities (a) and electrical double layer capacitances (b) of the 10 nm (curves (a)) and 200 nm (curves (b)) Pd electrodes. The simulations for the 10 nm electrodes have been performed, using Eqs. 18-22 and the continuity conditions given in Eq. 25. The numerical values of the parameters are also presented in Table I.

The simulated exchange current density for a 10 nm thick Pd electrode, shown in Fig. 6a (curve (a)) as a function of equilibrium potential of the MH electrode is also in good agreement with the experimental and theoretical results reported before by Notten *et al.* for AB_5-type materials [14,15]. α and Π_{ca} are calculated to be 0.27 and 0.545 eV, respectively. The activation energy is 0.481 eV (~46 kJ/mol), very similar to that of the 200 nm electrode.

The electrical double layer capacitances of the 10 nm electrode are approximately two times higher than that of the 200 nm electrode. The calculated double layer thicknesses are $d_{\theta}^{\alpha} = 0.606$ and $d_{1-\theta}^{\alpha} = 0.310$ nm for the α-phase, and $d_{\theta}^{\beta} = 0.401$ and $d_{1-\theta}^{\beta} = 0.239$ nm for the β-phase. The calculated limiting values for the specific double layer capacitance are $C_{MH}^{d}\big|_{\theta=0} = 2.24\times10^{-4}$ F/cm^2 and $C_{MH}^{d}\big|_{\theta=1} = 1.73\times10^{-4}$ F/cm^2 for the 10 nm electrode.

It is interesting to note that in the case of instantaneous phase transition (section III.C) it is impossible to identify the surface kinetic parameters only on the basis of the isotherm. That was shown before in Refs. [9,12]; the model equations then completely coincide with the basic LGM equations derived in Refs. [6,7]. The extra experimental information obtained from the impedance measurements, *i.e.* the exchange current densities and specific electrical double layer capacitances, is key to completely identify the electrochemical kinetics of MH-storage systems.

V. CONCLUSIONS

The recently presented Electrochemical Kinetic Model (EKM), describing the electrochemical hydrogen storage in hydride-forming electrodes, has been extended with the description of the solid/electrolyte interface, by including the charge transfer kinetics and electrical double layer charging. The model is based on first principles of (electro)chemical reaction kinetics and statistical thermodynamics. A complete set of equations has been derived, describing the equilibrium hydrogen partial pressure, equilibrium electrode potential, exchange current density and specific electrical double layer capacitance as a function of the hydrogen content in both solid-solutions and two-phase coexistence regions. In the final set of equations the exchange current density and specific electrical double layer capacitance are presented as functions of microscopic thermodynamic parameters, such as interaction energies between absorbed hydrogen atoms, electrochemical kinetic parameters (charge transfer coefficient), electrical double layer thicknesses. Combining statistical thermodynamics and electrochemical kinetics represents one of the advantages of the proposed approach.

Simulations of the experimentally measured electrochemical absorption isotherms, exchange current densities and specific electrical double layer capacities have been performed with Pd thin film electrodes with varying thickness. The model demonstrates a good agreement between the simulation results and experimental data. Many of the relevant parameters of the complex MH storage electrode system have been identified.

The proposed approach provides an explicit link between macroscopic parameters, which are often easily accessible experimentally (equilibrium potential, exchange current density etc.) and microscopic parameters (atomic interaction energies, *etc*.) which are more difficult, if not impossible, to access. A successful application of the proposed model to the complex Pd hydrogen storage system shows that the model is well suited to determine both the thermodynamics and kinetics of electrochemical hydrogen storage in hydride-forming materials.

VI. ACKNOWLEDGEMENTS

The authors wish to acknowledge financial support from Senter Novem (Subsidiebureau Energie Innovatie, the Netherlands, the proj. numb. NEOT05004).

REFERENCES

[1] Y. Fukai, *The Metal-Hydrogen System* (Springer-Verlag, Berlin, 2005).

[2] P.H.L. Notten, *Interstitial intermetallic alloys*, ASI Series Vol. E28, chapt. 7 (NATO, 1995).

[3] P.H.L. Notten, M. Latroche, *Nickel-Metal Hydride batteries: a successful application of hydrogen storage materials* (Encyclopedia of Electrochemical Power Sources, in press 2009).

[4] H.J. Bergveld, W.S. Kruijt, P.H.L. Notten, *Battery Management Systems, Design by Modelling* (Kluwer Acad. Publish., 2002).

[5]V. Pop, H.J. Bergveld, D. Danilov, P.P.L. Regtien, P.H.L. Notten, *Battery Management Systems, Accurate State-of-Charge Indication for Battery-Powered Applications* (Springer, 2008).

[6] A. Ledovskikh, D. Danilov, W.J.J. Rey, P.H.L. Notten, Phys. Rev. B, **73** (2006) 014106.

[7] P. Vermeulen, A. Ledovskikh, D. Danilov, P.H.L. Notten, J. Phys. Chem. B, **110** (2006) 20350.

[8] P. Vermeulen, A. Ledovskikh, D. Danilov, P.H.L. Notten, Acta Materialia, **57** (2009) 4967.

[9] A. Ledovskikh, D. Danilov and P.H.L. Notten, *Phys. Rev. B,* **76** (2007) 064106.

[10] E. Gileadi, B. E. Conway, *The Behavior of Intermediates in Electrochemical Catalysis in Modern Aspects of Electrochemistry*, N3, p. 347 (Butterworth, London, 1964).

[11] A. Ledovskikh, D. Danilov, P.H.L. Notten, Chem. Phys. Chem., **9** (2008) 1040.

[12] A. Ledovskikh, D. Danilov, P. Vermeulen and P.H.L. Notten, Electrochim. Acta, **55** (2009) 19.

[13] P. Kalisvaart, P. Vermeulen, A. Ledovskikh, D. Danilov and P.H.L. Notten, J. Alloys and Compounds, **446-447** (2007) 648.

[14] P.H.L. Notten, M. Ouwerkerk, A. Ledovskikh, H. Senoh and C. Iwakura, J. Alloys Comp. **356–357** (2003) 759.

[15] H. Senoh K. Morimoto, H. Inoue, Ch. Iwakura and P. H. L. Notten, *J. Electrochem. Soc.*, **147** (2000) 2451.

[16] R.A.H. Niessen and P.H.L. Notten, J. Electrochem. Soc., **152** (2005) A2051.

[17] R.A.H. Niessen and P.H.L. Notten, Electrochim. Acta, **50** (2005) 2959.

[18] M. Baldauf, and D.M. Kolb, Electrochim. Acta, **38** (1993) 2145.

[19] J. Horkans, J. Electroanal. Chem., **106** (1980) 245.

[20] B.A. Boukamp, Solid State Ionics, **18-19** (1986) 136.; B.A. Boukamp, Solid State Ionics, **20** (1986) 31.

[21] L. Schlapbach, *Surface properties and activation*, Topics in Applied Physics, p.15 (Springer-Verlag, Berlin, 1992).

[22] A.J. Bard and L.R. Faulkner, Electrochemical methods, fundamentals and applications (John Wiley & Sons, New York, 2001).

[23] C.A. Nijhuis, B.A. Boukamp, B.J. Ravoo, J. Huskens and D.N. Reinhoudt, J. Phys. Chem. C 2007, 111, 9799.

[24] H. Frieske and E. Wicke, Ber. Bunsenges. Phys. Chem., **77,** 48 (1973).

[25] R.A.H. Niessen, P. Vermeulen, P.H.L. Notten, Electrochim. Acta, **51(12)** (2006) 2427.

[26] J.N. Murrell, A.D. Jenkins, *Properties of Liquids and solutions*, 2nd Ed. (John Wiley & Sons, Chichester, England, 1994).

FIGURES AND TABLE CAPTIONS

Fig. 1. (a) Schematic representation of the electrochemical hydrogen storage process taking place at/in the MH electrode. (b) General reaction scheme, including the hydrogen dissociation-recombination reaction (1), the absorption-desorption reaction (2), the charge-transfer reaction (3) and the gas-electrolyte molecular hydrogen exchange reaction (4).

Fig. 2. Simulated (line) equilibrium potential and partial equilibrium hydrogen pressure and experimental data (symbols) [7,12] for a 200 nm Pd electrode at 25 ºC.

Fig. 3. Impedance spectra of a 10 nm thick Pd thin film electrode at various hydrogen concentrations.

Fig. 4. Measured (symbols) and calculated (line) exchange current density (i^0) for 200 nm Pd electrode at 25 ºC as a function of normalized hydrogen content (a) and equilibrium potential (b); partial exchange current density in the α-phase (curve (a)), in the β-phase (curve (b)) and the total exchange current density (curve (c)).

Fig. 5. Measured (symbols) and calculated (line) specific electrical double layer capacitance (C_{MH}^{d}) for a 200 nm Pd electrode at 25 ºC as a function of normalized hydrogen content (a) and equilibrium potential (b); partial specific electrical double layer capacitances in the α-phase (curve (a)), in the β-phase (curve (b)) and the total specific electrical double layer capacitance (curve (c)).

Fig. 6. Measured (symbols) and calculated (lines) exchange current densities (i^0) (a) and specific electrical double layer capacitance (b) for a 200 nm (curve (a)) and 10 nm (curve (b)) Pd electrode at 25 ºC as a function of equilibrium potential.

Table I. Simulated parameter values under equilibrium kinetic conditions for various Pd thin films at room temperature. Bold parameters are obtained by optimization.

N	Par	Dimension	Pd 200 nm film	Pd 10 nm film
1	x_{α}	[a]	0.156	0.141
2	x_{β}	[a]	0.664	0.141 [b]
3	E_{α}^{b}	eV[a]	-0.034	-0.299
4	E_{β}^{b}	eV[a]	-0.154	-0.039 [b]
5	$U_{\alpha\alpha}^{b}$	eV[a]	0.025	1.778
6	$U_{\beta\beta}^{b}$	eV[a]	0.183	-0.061
7	$U_{\alpha\beta}^{b}$	eV[a,b]	0.796	--
8	L	eV[a,b]	0.041	-0.018
9	B_{1}^{α}	[b]	11.85	0.033
10	B_{1}^{β}	[a,b]	9.566	0.033 [b]
11	B_{2}^{α}		**0.155**	**0.410**
12	B_{2}^{β}	[a,c]	1	0.410 [b]
13	B_{3}^{α}	[b]	0.254	0.096
14	B_{3}^{β}	[a,b]	0.280	0.096 [b]
15	P_{α}	Pa[a,c]	10^{5}	$4.04\cdot10^{1}$
16	P_{β}	Pa[a]	$1.95\cdot10^{3}$	$4.04\cdot10^{1}$ [b]
17	E_{α}^{0}	[a,c]	1	1 [c]
18	E_{β}^{0}	[a]	7.097	1 [b]
19	$U_{\alpha\alpha}^{s}$	eV	**-0.042**	**-0.038**
20	$U_{\beta\beta}^{s}$	eV	**-0.005**	-0.038 [b]
21	Π_{ca}	eV	**0.586**	**0.545**
22	α		**0.350**	0.270
23	$d_{1-\theta}^{\alpha}$	nm	**0.572**	**0.310**

24	d_{θ}^{α}	nm	**0.880**	0.606 [b]
25	$d_{1-\theta}^{\beta}$	nm	**0.524**	**0.239**
26	d_{θ}^{β}	nm	**0.780**	**0.401**

[a] Parameters are taken from the Lattice Gas Model [6] and Electrochemical Kinetic Model [12]

[b] Parameters are calculated from the continuity conditions;

[c] Parameters are set constant by normalization.

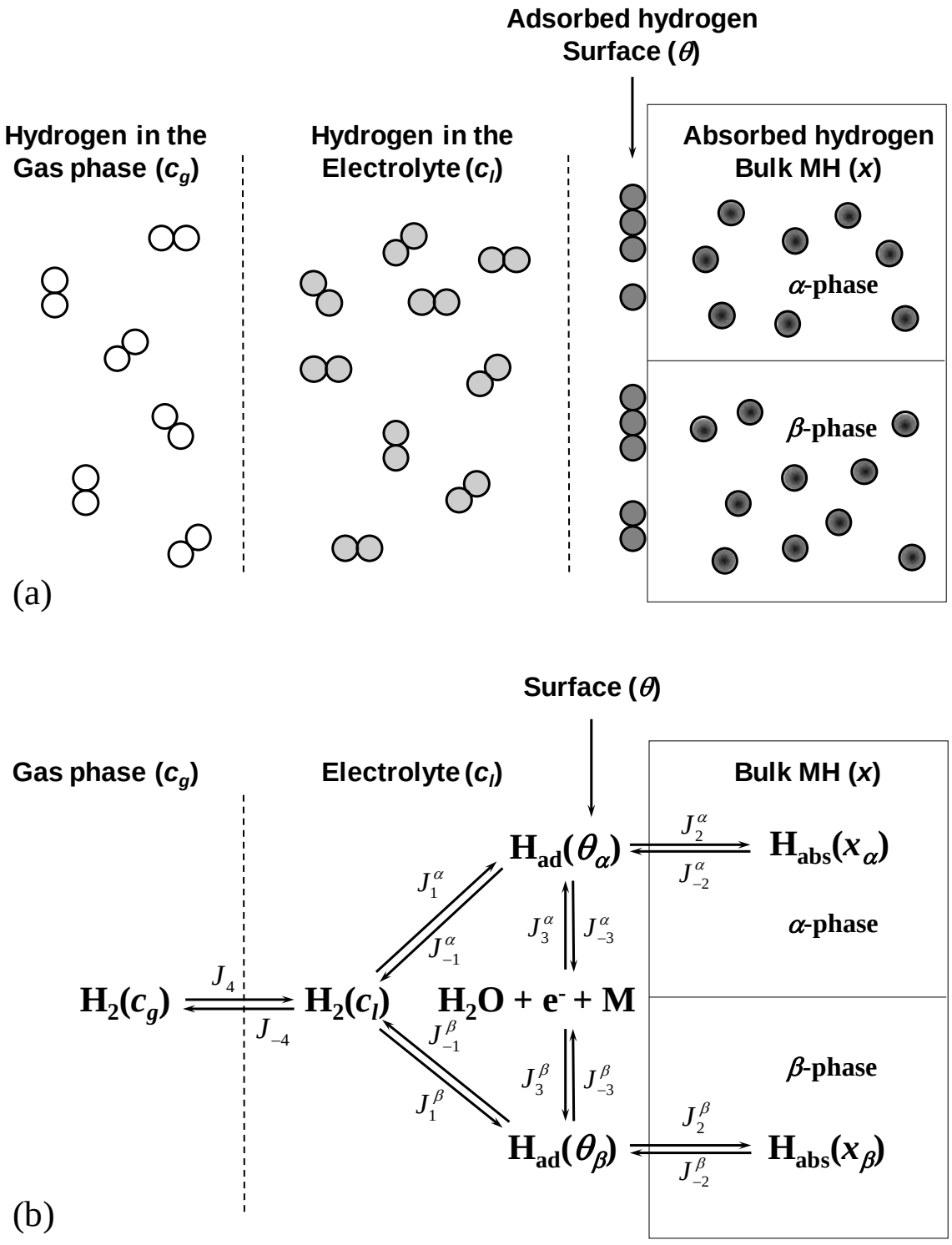

Fig. 1. (a) Schematic representation of the electrochemical hydrogen storage process taking place at/in the MH electrode. (b) General reaction scheme, including the hydrogen dissociation-recombination reaction (1), the absorption-desorption reaction (2), the charge-transfer reaction (3) and the gas-electrolyte molecular hydrogen exchange reaction (4).

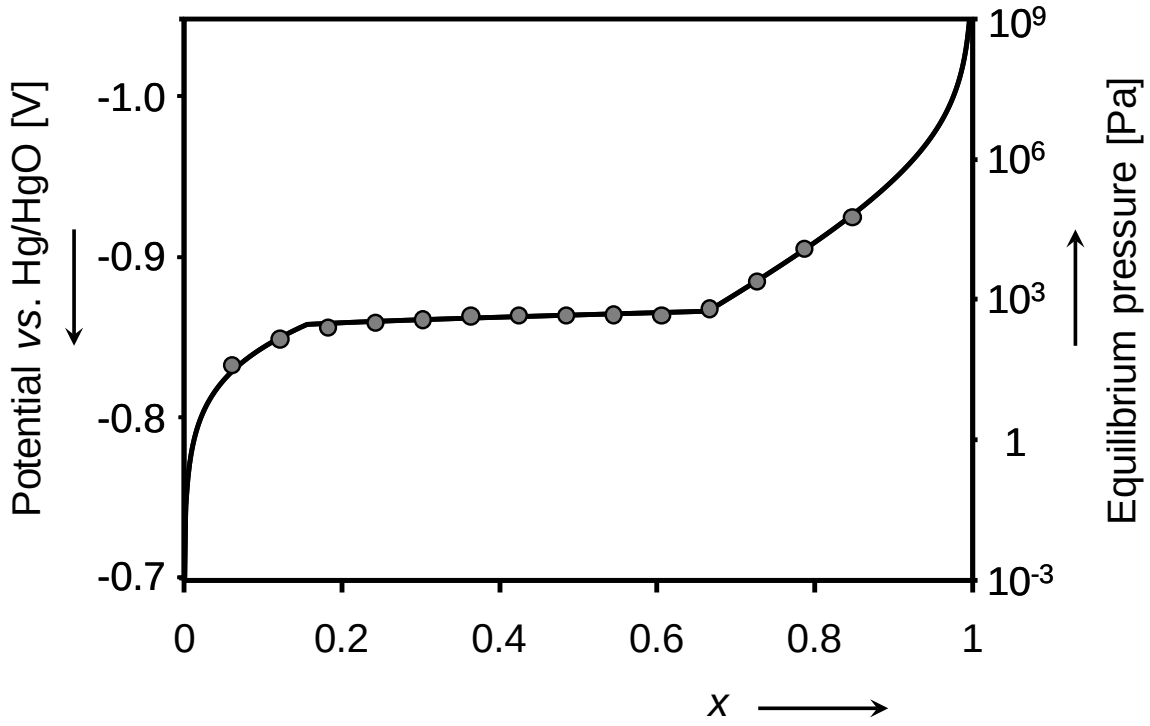

Fig. 2. Simulated (line) equilibrium potential and partial equilibrium hydrogen pressure and experimental data (symbols) [7,12] for a 200 nm Pd electrode at 25 ºC.

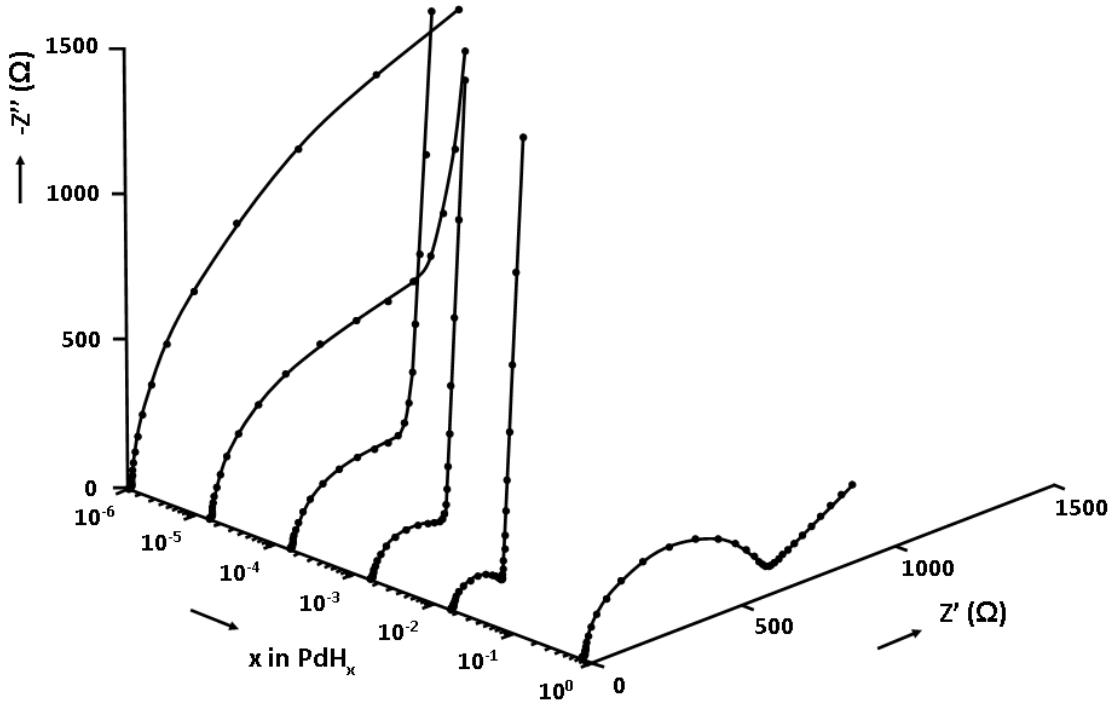

Fig. 3. Impedance spectra of a 10 nm thick Pd thin film electrode at various hydrogen concentrations.

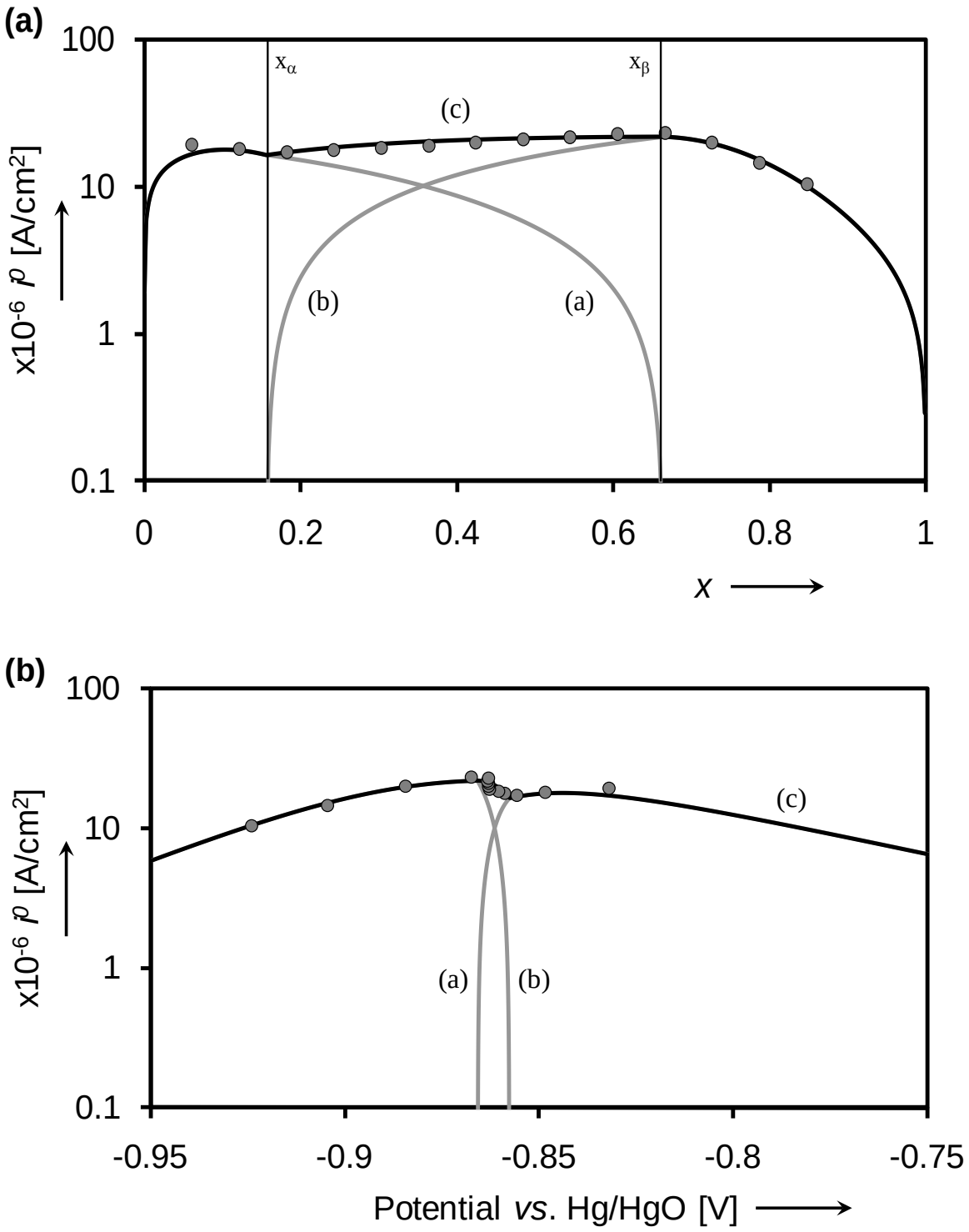

Fig. 4. Measured (symbols) and calculated (line) exchange current density (i^0) for 200 nm Pd electrode at 25 ºC as a function of normalized hydrogen content (a) and equilibrium potential (b); partial exchange current density in the α-phase (curve (a)), in the β-phase (curve (b)) and the total exchange current density (curve (c)).

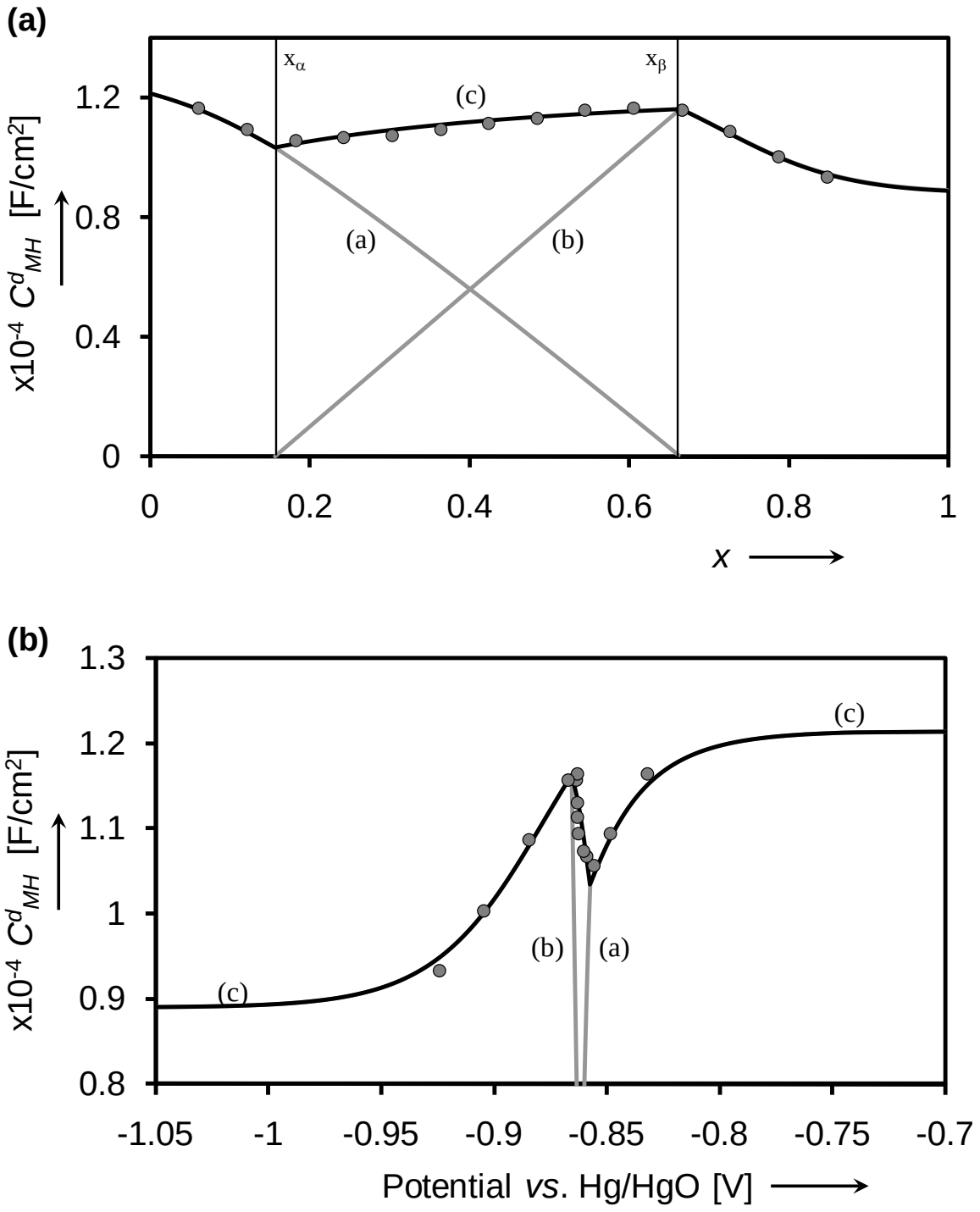

Fig. 5. Measured (symbols) and calculated (line) specific electrical double layer capacitance (C^d_{MH}) for a 200 nm Pd electrode at 25 ºC as a function of normalized hydrogen content (a) and equilibrium potential (b); partial specific electrical double layer capacitances in the α-phase (curve (a)), in the β-phase (curve (b)) and the total specific electrical double layer capacitance (curve (c)).

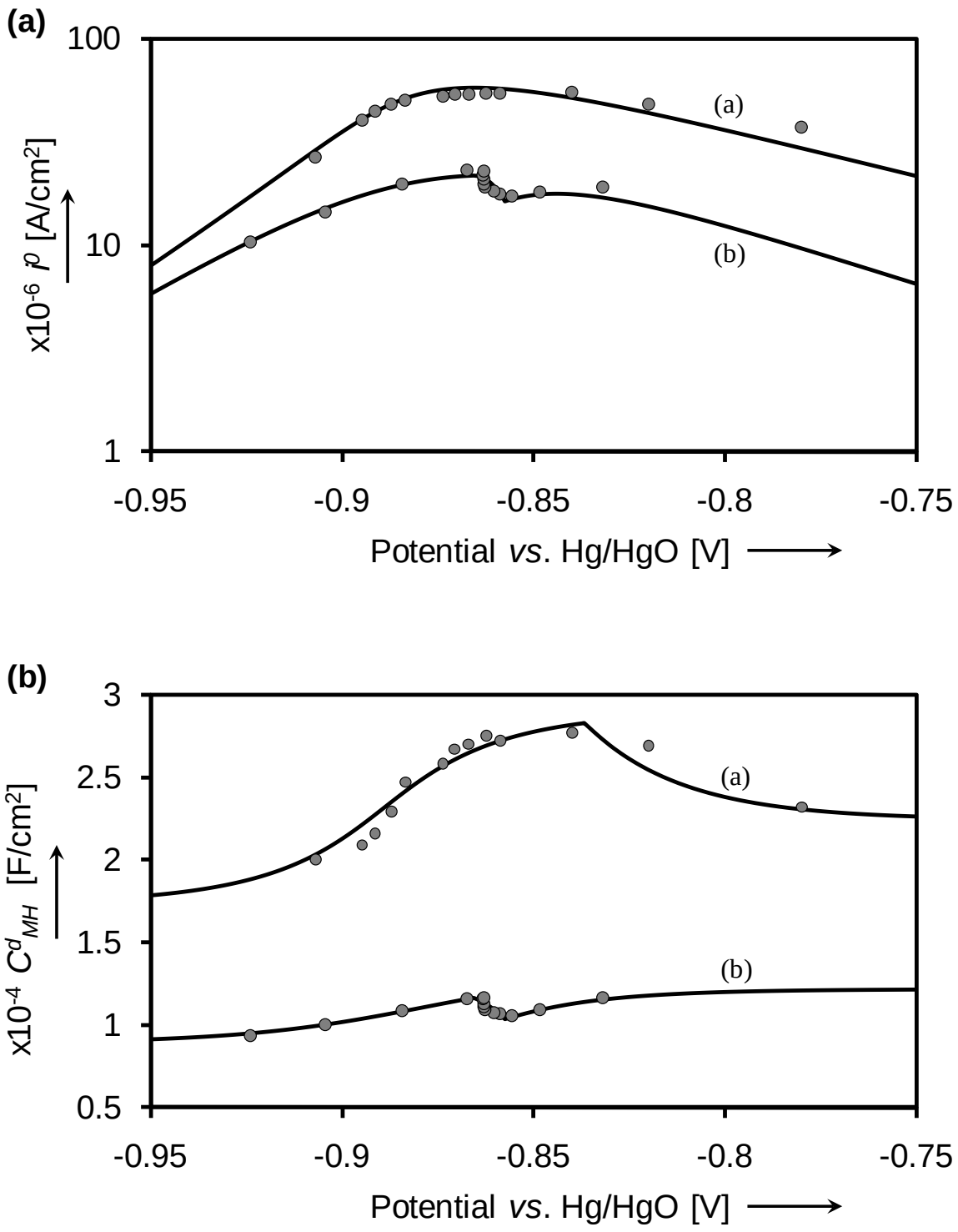

Fig. 6. Measured (symbols) and calculated (lines) exchange current densities (i^0) (a) and specific electrical double layer capacitance (b) for a 200 nm (curve (a)) and 10 nm (curve (b)) Pd electrode at 25 ºC as a function of equilibrium potential.